JOURNAL OF MAGNETIC RESONANCE **133,** 210–215 (1998)
ARTICLE NO. MN981464

Automated Shimming with Normal Spectrometer Hardware: 3D Profile Edge Shimming

Paul B. Chilvers and Gareth A. Morris[1]

Department of Chemistry, University of Manchester, Oxford Road, Manchester M13 9PL, United Kingdom

Received November 26, 1997

A novel method is proposed for automated magnetic field homogeneity adjustment in high-resolution NMR. The method uses measurements of the edge frequencies of slice profiles recorded under static gradients to obtain three-dimensional magnetic field maps and does not require significant extra spectrometer hardware. Results are presented for the ''cold'' shimming of 5- and 10-mm-diameter probes in a 400-MHz narrow bore magnet.

Key Words: **automated shimming; 3D shimming; field mapping; profile shimming; gradient shimming.**

The process of optimizing the homogeneity of the static magnetic field B_0 in high-resolution NMR spectroscopy wastes a great deal of instrument and operator time. This process of shimming is conventionally performed by manually adjusting the currents through a set of N appropriately shaped correction shim coils placed strategically about the field center (*1*). The object of the exercise is to find the combination of shim coil currents that generates the most uniform magnetic field across the volume of interest, a relatively straightforward problem of optimization in N dimensions. Despite the simple formulation of the problem, efficient automation of the shimming process has proved intractable until comparatively recently. One efficient general solution is to use a triple axis pulsed field gradient system to generate three-dimensional maps of the field imperfections and of the field shapes produced by each of the shim coils, and then to use iterative fitting to determine the set of shim coil currents that best correct the observed field inhomogeneity (*2*). This essentially requires that a high-resolution spectrometer be turned into a magnetic resonance imaging system, at considerable cost. This paper describes one possible method for performing full three-dimensional shimming without the need for additional hardware, using pulse sequences that do not require rapid switching of field gradients.

Until recently, most methods for automated shimming in high-resolution NMR relied on a single parameter as a criterion of field homogeneity, usually either the amplitude of a continuous wave lock signal or the integrated power of a free induction decay (*3*). A typical approach would be to use simplex optimization to seek the strongest lock signal achievable using a combination of a relatively small number of shim currents. Such methods were slow, showed poor convergence, and had a strong tendency to be seduced by local optima. The newer methods based on field mapping enjoy a much greater volume of information, typically using either a 1D or a 3D map of field distribution, and hence can be faster, more accurate, and more rapidly and more reliably convergent (*4–7*). These methods are descendants of those which have been used successfully for some time in magnetic resonance imaging (*8*). The most powerful approach demonstrated so far uses triple axis pulsed field gradients to provide a 3D field map based on the spatial dependence of the phase shifts generated by adding an extra precession period to a proton spin echo pulse sequence (*2*), but this requires expensive extra hardware, is best suited to samples with a strong single proton resonance, and requires separate mapping for each probe used. For practical high-resolution spectroscopy it is greatly preferable to use the deuterium lock resonance, since almost all samples can provide such a signal. For most samples it is also sufficient to shim only along the z axis, since this is the direction along which most of the sample-to-sample variation in field homogeneity is concentrated, and the effects of field variation orthogonal to z can be efficiently minimized by sample spinning. z axis shimming using the deuterium lock signal for single axis spin echo phase mapping has been shown to be highly efficient both in systems equipped with a z axis pulsed field gradient (*5, 6*) and in systems with only the slow ''homospoil'' facility to pulse the current through the z_1 shim coil (*6*).

Single-axis automated shimming methods are adequate for most purposes in routine high-resolution NMR spectroscopy, but there are two situations where full 3D shimming is essential and which typically lead to disproportionate amounts of time being spent on manual shimming. These two cases are where excellent instrumental lineshape is required for a static sample, for example, where an H_2O resonance must be suppressed, and where a new probe or magnet is to be commissioned. Since the former case is generally less difficult than the latter, it is the case of cold 3D shimming that will be concentrated on here. The purpose of the present paper is to examine the possibilities for automated cold 3D shimming without expensive extra hardwares and to demonstrate one method that can allow

[1] To whom correspondence should be addressed.

1090-7807/98 $25.00

automatic 3D shimming on many instruments with no significant hardware changes.

Field mapping by measuring the spatial dependence of spin echo phase shifts is highly effective, and with a suitable pulse sequence could be applied in three dimensions without the need for rapid field gradient switching. Unfortunately few modern spectrometers offer real-time control of any shim other than z_1, partly because of the modern tendency to rely on microprocessor-controlled shimming hardware. It is arguable that this enthusiasm for distributed intelligence has spread its intelligence too thinly: it would be possible to perform 3D phase mapping on older systems with real-time control of shim currents, despite the long settling times required. Without the ability to switch transverse field gradients during the course of a pulse sequence, an alternative strategy is required. One obvious approach is to use the information contained not in the phase but in the amplitude of a signal profile measured in the presence of a linear field gradient. The idea of ''profile shimming'' has been described previously, notably by Conover (*9*), and is in essence very simple. If a sufficiently large field gradient is applied that the net magnetic field changes monotonically as a function of distance along the gradient axis, then the frequency at which the integral of the signal reaches a given fraction of its total will correspond to the position at which the same fraction of the sample volume has been traversed: halfway up the integral corresponds to halfway across the sample.

Applied to z axis shimming in high-resolution spectroscopy, the quantitative implementation of amplitude profile shimming is not straightforward, since the signal measured as a function of z will depend in a complicated fashion on the choice of pulse sequence and on the variation of radiofrequency field strength B_1 along the sample. In the transverse plane, however, the signal profile as a function of position is defined very accurately by the use of a precision cylindrical sample tube. For a sample of radius r, and mapping along a read gradient axis q at right angles to z, if the small transverse B_1 inhomogeneity can be neglected then the relative signal integral as a function of position is given by

$$I(q) = q\sqrt{r^2 - q^2} + r^2\sin^{-1}(q/r) + \pi r^2/2, \qquad [1]$$

where q is the displacement from the sample center. Thus by measuring the signal profile $S(\nu)$ under a transverse field gradient G_q, the relationship between position and frequency can be found by inverting the function I:

$$q(\nu) = I^{-1}\left(\int_{-\infty}^{\nu} S(\nu)d\nu\right). \qquad [2]$$

Figure 1 illustrates this process diagrammatically, for an experimental signal profile across a 5-mm NMR tube.

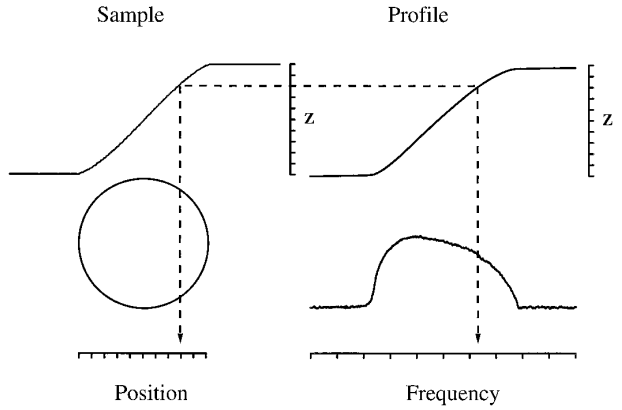

FIG. 1. Relationship between the integral of the sample spin density and the integral of a spectrum measured under a strong linear gradient. A profile was measured through a 5-mm sample of $CHCl_3$ in $CDCl_3$ on a 300-MHz Varian INOVA instrument, using the pulse sequence of Fig. 2 with z gradient pulses provided by the homospoil facility and a constant x gradient of approximately 0.04 G cm^{-1}. A time shift of approximately 4 ms was used to allow for the slow rise and fall of the homospoil pulse. Other experimental parameters were similar to those given in the main text for Figs. 4 and 5.

In principle, by measuring profiles along a range of directions q for different z positions it should be possible to construct a 3D map of sample frequency as a function of position. The process of analysis would not be straightforward, however, because of the difficulty of extracting unambiguously the required information about the signal frequency in the absence of an applied field gradient from the profiles measured in the presence of such a gradient. Problems arise because for any individual direction q there are many possible field distributions that would give rise to the same amplitude profile; only when a complete set of profiles sampling all directions q is available can the ambiguities be resolved, a process analogous to the use of projection–reconstruction algorithms in magnetic resonance imaging. Rather than proceed to try to extract all of the information potentially available from the profile amplitudes, it is sufficient to note that no ambiguity arises at the extreme edges of the spectrum: the frequency at the edge of the spectrum is the frequency at the edge of the sample. By recording the frequencies of the edges of the profiles as a function of gradient direction and of z position, it is possible to build up a 3D map of frequencies at points on a cylinder around the inside surface of the sample.

Figure 2 shows a practical pulse sequence for acquiring z-selective profiles in the presence of a small constant transverse field gradient G_q, chosen to give a profile at least 10 times wider than the unshimmed line. G_q may be large or small compared to the final required shim gradients, depending on the quality of the raw B_0 field. The selectivity needed in the z direction can be achieved by applying a selective refocussing pulse under a z field gradient in a spin echo sequence; the z position of the slice through which the profile is to be taken is determined by the frequency offset $\Delta\nu$ of the 180° pulse. A typical slice width corresponds to about 10% of the active signal volume; much less

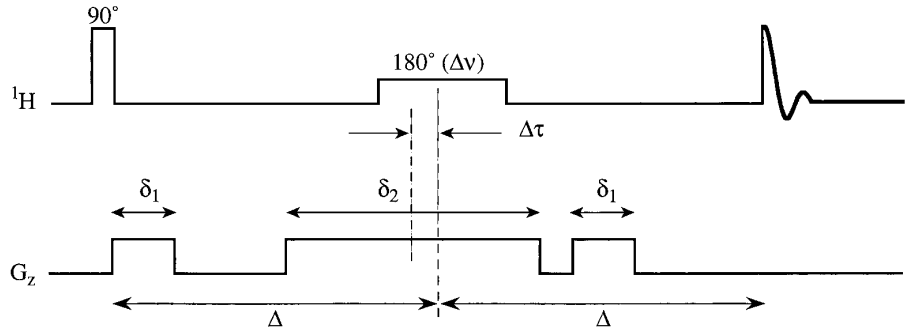

FIG. 2. Pulse sequence for measuring a *z*-selective signal profile in the presence of a weak transverse field gradient. Normal EXORCYCLE phase cycling (*10*) is used; the delays Δ are sufficient to ensure that perturbations of the static field B_0 by the gradient pulses have died away. Where the *z* gradient pulses have a slow response (e.g., if *z* shim homospoil pulses are used), the central gradient pulse must be moved backward in time to allow for finite rise and fall times. The exact timing of the onset of data acquisition is adjusted to minimize frequency-dependent phase shifts, and the timing of the change in transmitter frequency is chosen to minimize the dependence of signal phase on the offset $\Delta\nu$.

would impair sensitivity, much more would slow convergence and degrade the accuracy of mapping for higher order axial gradients. As with any spin echo pulse sequence, reasonable care should be exercised in calibrating both pulses. Provided that the pulsed *z* gradient is much larger than the small transverse gradient G_q applied, the tilt of the selected slice away from the *xy* plane because of the presence of G_q may be neglected. Because good signal-to-noise ratio is needed if the edge frequencies of the signal profile are to be determined accurately, this type of amplitude mapping is best applied to samples with a strong proton signal. Problems with radiation damping can be avoided by using two extra gradient pulses to ensure that the full proton magnetization only remains transverse for a short time. Where a *z* gradient with long rise and fall times (as is the case for homospoil pulses) is used, the timing of the field gradient pulse with respect to the refocussing pulse will need empirical optimisation. The second half of the spin echo is recorded and Fourier transformed to give a phase-sensitive amplitude profile; long echo times may be necessary where slow gradient pulses are used, in order to avoid perturbations caused by field disturbances and eddy current effects. EXORCYCLE phase cycling (*10*) is desirable where time averaging is used.

The analysis of the experimental data in edge frequency mapping is much simpler than in full 3D amplitude profile mapping. If profiles are recorded under two equal and opposite field gradients G_{+q} and G_{-q}, which are both strong compared to the field inhomogeneity, then if the lower frequency limit for the $+q$ profile corresponds to the left-hand edge of the sample, the same point will correspond to the upper frequency limit of the $-q$ profile, and vice versa for the right-hand edge. Thus the average of the lower frequency limit for the $+q$ profile and the upper frequency limit for the $-q$ profile will be the frequency at one edge of the sample in the absence of an applied gradient, and the average of the upper frequency limit for the $+q$ profile and the lower frequency limit for the $-q$ profile will be the frequency at the other, as shown in Fig. 3.

Two factors complicate the extraction of edge frequencies: the limitations imposed by noise, and systematic errors in the signals measured. The former issue is best dealt with by using the signal integral as a criterion: the ''edges'' of the signal profile are taken to be where the signal integral crosses (say) the 5% and the 95% thresholds. The closer the thresholds are set to 0 and 100%, the closer the frequencies determined become to the true edge frequencies, but the more susceptible the measured frequencies are to systematic errors. The latter include phase variation with read gradient orientation *q* and position *z*, baseline offsets, and lineshape disturbances caused by spurious echoes. Phase variations can be reduced (but not eliminated) in practice by adjusting the timing of data acquisition and of the frequency shift $\Delta\nu$, and the effects of residual phase errors can be suppressed by automatic zero-order phase correction of the profiles. Baseline errors can again be minimized by appropriate choice of pulse sequence timing, with residual errors corrected by software. In practice the phase and baseline correction can be carried out using a simultaneous optimization. Spurious echoes arise when the off-resonance effects of the selective and nonselective pulses are partly refocused by the field gradients; the echoes are generally small but occasionally troublesome. These echo effects disappear as the field homogeneity improves and do not greatly interfere with the convergence of automated shimming, but a more elegant approach might be to use two selective refocusing pulses rather than one, canceling the offset (and hence *z*) dependence of the phase of the refocused signal.

Having established a viable method for sample edge frequency mapping, automated 3D shimming requires that sufficient measurements be made to map the magnetic field adequately. The number of edge frequency measurements made will determine the order of correction obtainable: in principle any number of shims can be optimized provided sufficient points are measured. Too few measurements will fail to characterize all the gradients that could be corrected with a given set of *N* shim coils, and will show poor convergence to an optimum solution; too many measurements will be expensive in time. Two diametrically opposed points are determined for each pair of experimental profiles; a simple strategy for selecting mapping points is to seek a helical

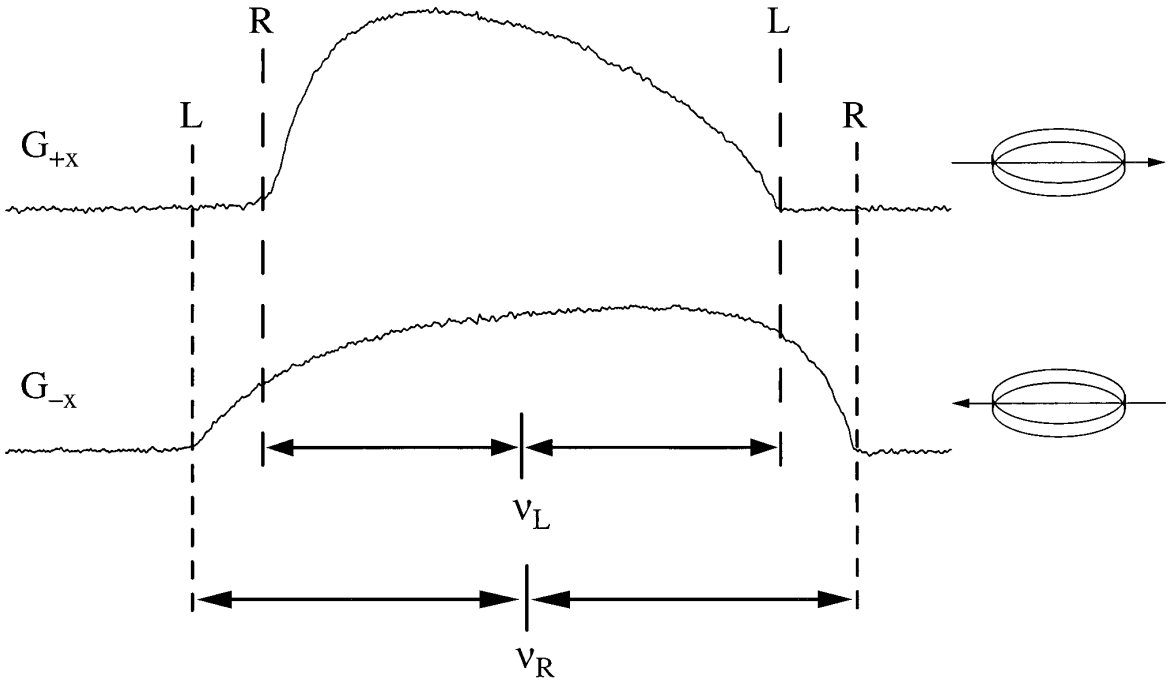

FIG. 3. Illustration of the calculation of the frequencies at the edge of a cylindrical sample using two profiles measured using (top) a positive and (bottom) a negative field gradient. For linear applied gradients the frequency ν_L at the left-hand edge of the sample in the absence of an applied gradient is the average of the two frequencies marked L, and ν_R at the right-hand edge is the average of the frequencies marked R.

sampling pattern in which these pairs of points are distributed approximately evenly over the surface of the sample. The minimum number of sampling points required to allow the settings of N shims to be determined is in principle $N + 1$, but because of the need for a compromise between approximately uniform sampling of the sample surface (to ensure best homogeneity over all the sample) and the need to sample sufficiently finely (in order to determine the best settings for high order shims), practical experiments sample significantly more points. The helical sampling pattern lends itself readily to automation, since the desired conditions can be established simply by incrementing linearly the offset $\Delta\nu$ of the selective 180° pulse and the angle θ made by the read gradient q with the x axis.

For a set of M pairs of profiles covering a helix of h turns and length Δz, the ith pair of profiles will have a frequency offset for the selective 180° pulse of

$$\Delta\nu = \left(\frac{2i - 1 - M}{2M - 2}\right)\left(\frac{\gamma G_z \Delta z}{2\pi}\right) \qquad [3]$$

and transverse gradients

$$G_{+x} = +G_r \cos\left\{2\pi h\left(\frac{2i - 1 - M}{2M - 2}\right)\right\}$$

$$G_{+y} = +G_r \sin\left\{2\pi h\left(\frac{2i - 1 - M}{2M - 2}\right)\right\} \qquad [4]$$

for one profile and

$$G_{-x} = -G_r \cos\left\{2\pi h\left(\frac{2i - 1 - M}{2M - 2}\right)\right\}$$

$$G_{-y} = -G_r \sin\left\{2\pi h\left(\frac{2i - 1 - M}{2M - 2}\right)\right\} \qquad [5]$$

for the other, where the transverse read gradient is of magnitude G_r and the longitudinal gradient used for z slice selection is G_z.

Once a complete set of M pairs of profiles has been acquired for the current state of the B_0 field, a further series of N sets of profiles can be measured in which each of the N shim currents is offset in turn. Extracting the $2M$ edge frequencies ν_i^0 from the $2M$ profiles in the first set gives a 3D map describing the spatial dependence of the raw B_0 field; the edge frequencies ν_i^j measured from the remaining N sets of profiles describe the spatial dependence of B_0 with each in turn of the shim currents changed. Representing the raw B_0 field map as a vector $\mathbf{F}^o = (\nu_1^0, \nu_2^0, \ldots, \nu_{2M}^0)$, a set of N shim maps $\mathbf{S}^j = (\nu_1^j, \nu_2^j, \ldots, \nu_{2M}^j) - \mathbf{F}^o$ can be constructed which describe the shapes of the fields generated by each of the shim coils. If the starting set of shim currents is represented by a vector $\mathbf{I}^o = (I_1, I_2, \ldots, I_N)$ then a vector $\Delta\mathbf{I}^o = (\Delta I_1^o, \Delta I_2^o, \ldots \Delta I_N^o)$ may be defined which consists of the changes made to each of the shim currents when constructing the shim maps. The information obtained on the dependence of field shape on shim currents is then summarized

by the matrix B whose columns are the vectors $\mathbf{S}^j$ divided by the appropriate component of $\Delta\mathbf{I}^o$:

$$B_{ij} = (\nu_i^j - \nu_i^0)/\Delta I_j^o. \quad [6]$$

The problem of shimming then reduces to using the information contained in B to find a correction to the shim currents **I** that will make the components of the field map **F** as near equal as possible. This is a standard problem in least squares fitting, to which algorithms such as singular value decomposition (*11*) are well suited. Once a correction vector $\Delta\mathbf{I}^c$ has been calculated from the starting field map $\mathbf{F}^o$, the shim currents can be set to incorporate this change and a second map $\mathbf{F}^1$ can be measured and a second correction vector calculated using the matrix B, and so on until a sufficiently flat field map has been obtained. In practice, any instrument on which such a scheme can be implemented will also be capable of performing phase profile mapping along the *z* axis (*6*), using either a rapid pulsed field gradient system or a homospoil. Since phase profile mapping is both quicker and more convergent than edge frequency mapping, it is generally more efficient to interleave cycles of 3D edge profile mapping and *z* phase mapping than to rely purely on edge profile mapping.

The procedures described were implemented on two Varian INOVA instruments, a 400-MHz spectrometer with *z* pulsed field gradient facilities, and a 300-MHz spectrometer with only a homospoil, using the pulse sequence of Fig. 2. The only hardware modifications to the two instruments were the addition of automatic radiofrequency switching for convenience when using deuterium *z* phase profile shimming, and a change to the value of one capacitor in the homospoil duration limit circuitry of the shim current controller (*6*). Software for the analysis of the profile data was implemented in C within the Vnmr software package, using the approach described above with the singular value decomposition algorithm of Ref. (*11*). Samples with strong proton signals were used, as discussed earlier, with deuterated solvents included to allow automated *z* axis shimming using the method of Ref. (*6*). Both systems used a 13-channel shim set, with nominal shapes z^1, z^2, z^3, z^4, z^5, x, y, xy, x^2-y^2, xz, yz, x^3, and y^3.

Figure 4 shows cold shimming results obtained at 400 MHz using a 5-mm indirect detection probe. 3D shimming was performed using a strong proton signal from dioxane in $CDCl_3$, with TMS added as a linewidth standard. A 6-turn helical sampling scheme with 29 pairs of points covering a *z* displacement of approximately 12 mm was used. Two transients were recorded for each profile, with a spectral width of 200 Hz, a data acquisition time of 5.12 s, a recycle time of 7.12 s, and a delay Δ of 100 ms. A simple rectangular soft 180° pulse of duration 840 μs was used, with a *z* field gradient of 2.74 G cm^{-1} produced using the actively shielded gradient coil of the probe and the Varian Performa II gradient amplifier, giving a profile slice thickness of approximately 1.9 mm. The transverse read gradient, provided by the normal shim coils, was approximately 0.06 G cm^{-1}. The central

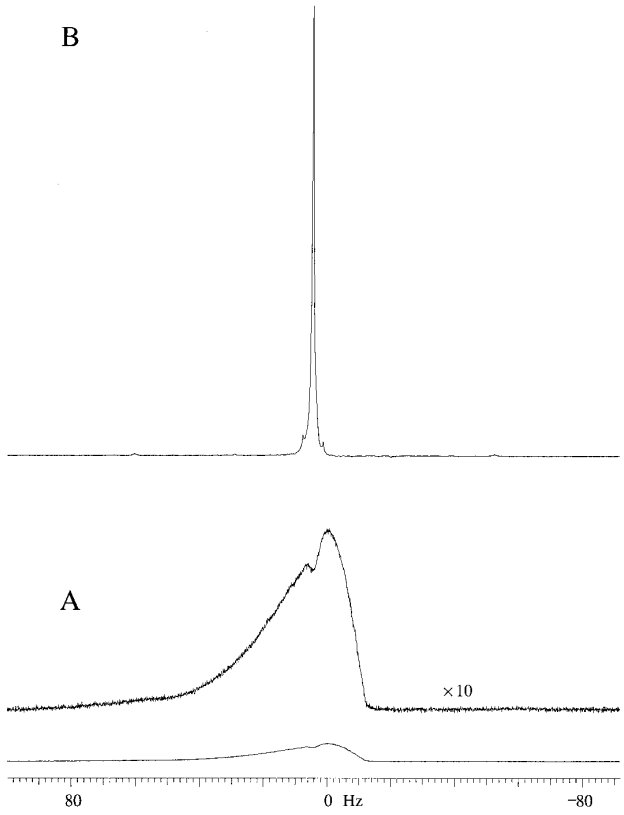

FIG. 4. ^{1}H lineshape of TMS, obtained at 400 MHz using a 5-mm indirect detection probe, for a nonspinning sample of dioxane and TMS in $CDCl_3$. A: Lineshape with all shim currents set to zero. B: Lineshape after 17 interleaved cycles of 1D *z* phase shimming and 3D profile shimming; full linewidth at half height is 0.6 Hz.

field gradient pulse was of duration δ_2 = 2.84 ms, and the two shorter *z* gradient pulses δ_1 for the reduction of radiation damping effects, of equal amplitude 2.74 G cm^{-1}, were both 1 ms. At the start of the experiment all the currents through the room temperature shim coils were set to zero, and shim maps for both 1D *z* phase profile shimming and 3D proton profile edge frequency shimming were measured. Interleaved cycles of automated 1D *z* shimming (z^1 to z^5 only) and 3D shimming were carried out until satisfactory convergence was obtained. In total, 14 cycles of *z* and 3 cycles of 3D shimming were used; the final result was a nonspinning proton linewidth of 0.6 Hz, as shown in Fig. 4A, obtained in a total time of approximately 3.5 h.

Figure 5 shows results obtained at 400 MHz using a 10-mm broad band probe without pulsed field gradient facilities. 3D shimming was performed using the proton signal from 40% dioxane in C_6D_6. The same sampling scheme was used as for Fig. 4, but in this case the 3D shim maps for z^1, z^2, x, y^1, xz, yz, xy, x^2y^2, x^3, and y^3 were measured with close to optimum shim settings, in a time of approximately 12 h; using shim maps obtained with optimized shims speeds convergence slightly. Eight transients per profile were recorded, with a spectral width of 400 Hz, an acquisition time of 5.12 s, a recycle time of 7.12 s, and a delay τ of 400 ms. A longer Δ

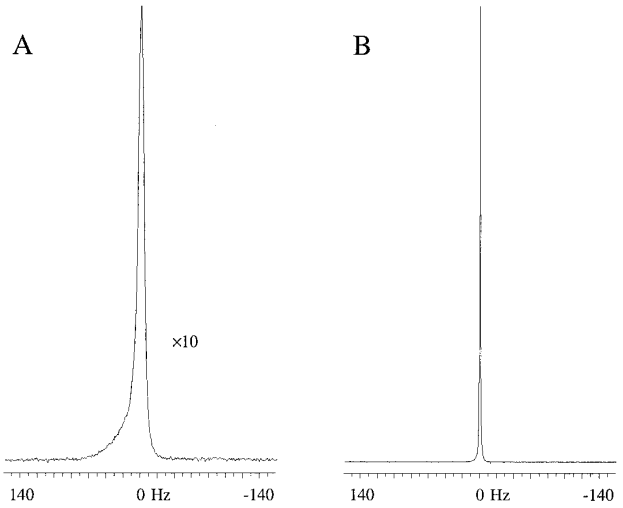

FIG. 5. ^{13}C lineshape of C_6D_6 from a nonspinning 40% dioxane/60% C_6D_6 sample, measured at 400 MHz using a 10-mm broad band probe. A: Lineshape with all shim currents set to zero. B: Lineshape after 17 cycles of 1D *z* phase shimming and 3D profile shimming; full linewidth at half height is 0.6 Hz.

delay than for the 5-mm probe was required since the homospoil, which has long rise and fall times, was used to produce the *z* field gradient for the 10-mm probe. A rectangular soft 180° pulse of duration 9 ms was used, with a *z* field gradient of 0.35 G cm^{-1} produced by the homospoil facility, giving a profile slice thickness of approximately 1.5 mm. The transverse read gradient, provided by the normal shim coils, was approximately 0.05 G cm^{-1}. The central field gradient pulse was of duration $\delta_2 = 32$ ms, but displaced from the center of the selective 180° pulse by $\Delta\tau = 6.5$ ms, to account for the relatively long rise and fall times of the homospoil. To reduce the effect of radiation damping the two shorter homospoil pulses used were of duration $\delta_1 = 5$ ms. Prior to cold shimming, maps of shims z^1 to z^5 were obtained with optimum shim settings, using 1D *z* shimming. At the start of the shimming procedure all shim gradients were set to zero, then interleaved cycles of 1D *z* shimming and 3D profile shimming were carried out until the best convergence was found. For the 3D shimming one transient per profile was acquired, giving a time of 7.3 min per cycle. In total, 14 cycles of *z* and 3 cycles of 3D shimming were used, producing a nonspinning ^{13}C linewidth of 0.6 Hz in a time of 40 min. The total time required, including acquisition of the map data, was a little over 12 h. The linewidth measured with the same shim settings but with the sample spinning at 12 Hz was 0.15 Hz.

The results shown in Figs. 4 and 5 were at least as good as those previously produced by extended manual shimming, suggesting that both for cold shimming on installation and for 3D shimming on critical nonspinning samples it is indeed a practical proposition to perform full automated shimming without using a triple axis rapid pulsed field gradient system. There is considerable scope for improving both the speed of convergence of the technique described and the quality of the end results obtainable; in its present form it uses only the profile edge frequencies, which are a small fraction of the total information available from the profiles. The principle of 3D shimming with modest instrumental resources having been established, however, another attractive proposition is to examine the minimum hardware requirements for 3D phase profile shimming. It should be possible to perform 3D phase mapping using pulsed *x* and *y* shim coil currents, despite their low amplitude and slow response, if hardware for their real-time control can be implemented. This would greatly reduce the time and sensitivity demands of 3D automated shimming at modest cost. Work is now being done on the testing of such an approach.

ACKNOWLEDGMENTS

Helpful discussions with Hervé Barjat and Bayard Fetler are gratefully acknowledged. This work was supported by the EPSRC Grants GR/L17443 and GR/K44619. G.A.M. gratefully acknowledges receipt of a Research Fellowship from the Leverhulme Trust.

REFERENCES

1. W. A. Anderson, *Rev. Sci. Instrum.* **32,** 241 (1961).
2. P. C. M. van Zijl, S. Sukumar, M. O'Neil-Johnson, P. Webb, and R. E. Hurd, *J. Magn. Reson. A* **111,** 203 (1994).
3. W. W. Conover, *in* ''Topics in Carbon-13 NMR'' (G.C. Levy, Ed.), Vol. 4, Chap. 2, Wiley, New York (1984).
4. S. Sukumar, M. O'Neil-Johnson, and J. A. B. Lohman, 37th Experimental NMR Conference, Asilomar, 1996.
5. S. Sukumar, M. O'Neil-Johnson, R. E. Hurd, and P. C. M. van Zijl, *J. Magn. Reson. A* **125,** 159 (1997).
6. H. Barjat, P. B. Chilvers, B. K. Fetler, T. J. Horne, and G. A. Morris, *J. Magn. Reson. A* **125,** 197 (1997).
7. G. A. Gray and B. K. Fetler, ''Magnetic Moments,'' Vol. VIII, No. 1, p. 16, Varian Associates, Palo Alto (1996).
8. M. G. Prammer, J. C. Haselgrove, M. Shinnar, and J. S. Leigh, *J. Magn. Reson.* **77,** 40 (1988); C. Pedersen, N. Bansal, and R. L. Nunnally, *Radiology* **173P,** 380 (1989); J. Tropp, K. A. Derby, and C. Hawrysko, *J. Magn. Reson.* **85,** 224 (1989); E. Schneider and G. Glover, *Magn. Reson. Med.* **18,** 335 (1991); P. Webb and A. Macovski, *Magn. Reson. Med.* **20,** 113 (1991); S. Kanayama, S. Kuhara, and K. Satoh, *Magn. Reson. Med.* **36,** 637 (1996).
9. R. C. Crouch, A. O. Davis, A. Ragouzeous, and G. A. Gray, ''Magnetic Moments,'' Vol. VII, No. 1, p. 23, Varian Associates, Palo Alto (1995); W. W. Conover, *in* ''Topics in Carbon-13 NMR Spectroscopy,'' (G. C. Levy, Ed.), Vol. 4, Chap. 2, Wiley, New York, 1984.
10. G. Bodenhausen, R. Freeman, and D. L. Turner, *J. Magn. Reson.* **27,** 511 (1977).
11. W. H. Press, B. P. Flannery, S. A. Teukolsky, and W. T. Vetterling, ''Numerical Recipes in C,'' Cambridge Univ. Press, Cambridge, UK, 1988.